DOI: 10.1002/cphc.200900246

Applications of the Static Quenching of Rhodamine B by Carbon Nanotubes

Ashraf Ahmad,*[a] Tetiana Kurkina,[a] Klaus Kern,[a, b] and Kannan Balasubramanian*[a]

We report here on the interaction of the fluorescent dye rhodamine B (RB) with single-walled carbon nanotubes (SWCNTs). We observe that SWCNTs statically quench the fluorescence of RB by forming a stable ground state complex. Careful spectroscopic analysis indicates that the complex formation is efficient mainly with certain chiral forms. We propose three different applications utilizing this quenching mechanism and the associated complexation. Firstly, the quenching efficiency can be utilized as a measure for the characterization and quantification of nanotube dispersions. Secondly, we demonstrate that the specific complexation of RB can be deployed to enrich certain chiral forms in suspension. Finally, we show that RB can be effectively used to visualize nanotubes deposited on substrates.

1. Introduction

Single-wall carbon nanotubes (SWCNTs) are a class of nanomaterials that is extensively investigated due to their unique physical and chemical properties. One of the major hurdles for their widespread application is the non-availability of monodisperse SWCNTs.[1] Most of the production methods such as arc discharge,[2] laser ablation,[3] chemical vapor deposition,[4] high pressure pyrolysis (HiPCO)[5] and Co/Mo catalyst process (CoMoCAT)[6] produce a mixture of different tube diameters and lengths. Methods for separating a single chiral form from the raw material suffer from the difficulty to characterize the tube dispersions accurately at various separation stages. A number of techniques are being developed to overcome this problem, among which near-infrared spectroscopy together with Raman spectroscopy are being widely used.[7] Although these techniques are able to determine the composition of nanotube dispersions to a large extent, complete information about the dispersion is not yet routinely possible. A simple, powerful and fast characterization technique is still being sought for. In the present study, we found that SWCNTs statically quench rhodamine B (RB) through the formation of a ground state complex (Figure 1) with some chiral forms. Based on such static quenching, we propose a novel method for SWCNT quantification and characterization, which is analogous to the use of nucleobase-specific fluorescence quenching for DNA sequencing.[8] In addition, specific complexation was evaluated as a tool for the visualization of SWCNTs by confocal microscopy and for the partial purification of tube dispersions.

2. Results and Discussion

The addition of SWCNTs to a dye solution leads in general to a reduction in the fluorescence intenisity of the latter.[9–11] Quenching of dye photoluminescence requires close proximity between the quencher and the dye. Depending on the chemical nature of the dye and its interaction, two types of quenching may occur: collisonal/dynamic and static quenching.[12] In the former case, the quencher must diffuse to the fluorophore during the lifetime of the excited state. In many cases, energy transfer might also occur from the fluorophore on to the quencher through long-range dipole–dipole interactions.[9–11,13–15] The intrinsic physical and chemical properties of both the species remain unchanged through this interaction.[9,16] By contrast, in static quenching, hydrophobic and electrostatic interactions lead to the formation of a non-fluorescent ground-state complex between the fluorophore and the quencher with new physical and/or chemical properties.[12,16] Apart from quenching phenomena, charge transfer based donor–acceptor interactions might also occur.[17–20]

Rhodamine B (RB) belongs to a family of fluorone dyes that all share the same basic fluorone skeleton (Figure 1 A). Addition of SWCNTs to RB solution led to a drastic reduction in the fluorescent intensity of RB (FI) compared to the initial fluorescent intensity (FI^0) in the absence of SWCNTs (Figure 1 B). The fluorescence emission spectra of RB in the presence of various quantities of nanotube raw material are summarized in Figures 2 and 3 for CoMoCAT and HiPCO SWCNTs respectively. It is apparent that as the concentration of nanotubes increases, the emission from RB continuously decreases. The Stern–Volmer plots[21] (FI^0/FI as a function of tube concentration) shown in the insets of the figures are found to be non-linear with an upward curvature. While the quenching pattern in both cases

[a] Dr. A. Ahmad, T. Kurkina, Prof. K. Kern, Dr. K. Balasubramanian
Max Planck Institute for Solid State Research
Heisenbergstr. 1, D-70569 Stuttgart (Germany)
Fax: (+49) 711 689-1662
E-mail: a.ahmad@fkf.mpg.de
B.Kannan@fkf.mpg.de

[b] Prof. K. Kern
Institut de Physique des Nanostructures
Ecole Polytechnique Fédérale de Lausanne
CH-1015 Lausanne (Switzerland)

Supporting information for this article is available on the WWW under http://dx.doi.org/10.1002/cphc.200900246.

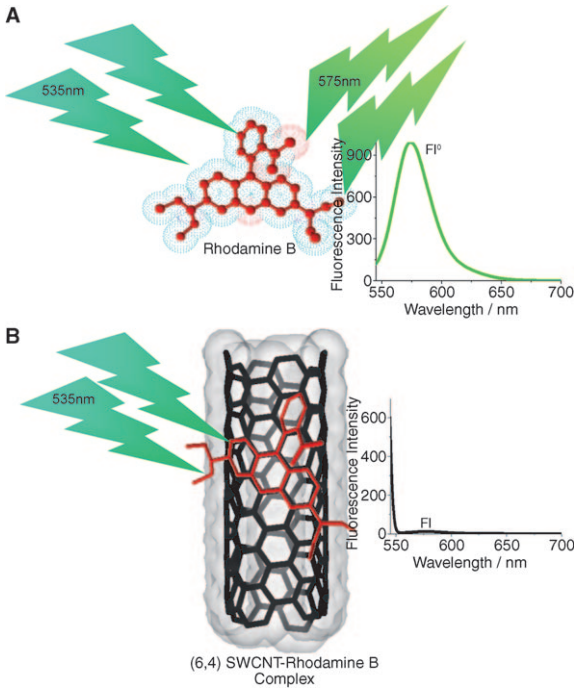

Figure 1. Schematic showing the quenching of RB fluorescence by SWCNTs. A) RB chemical structure prepared by using ACD/ChemSketch (Advanced Chemistry Development, Inc.) showing the basic fluorone skeleton. On the right, the fluorescence emission spectrum from free RB in solution is shown. B) Structure of SWCNT-RB complex along with the emission spectrum showing significant quenching of RB fluorescence by the nanotubes. (6,4) chiral form was constructed using discovery studio visualizer (Accelrys Ltd.).

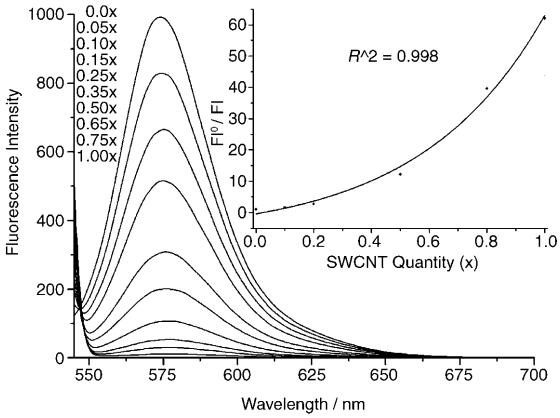

Figure 2. Emission spectra of 0.42 μM (final concentration) RB in the presence of different quantities of CoMoCAT nanotubes (excitation wavelength: 535 nm). 1x refers to the starting concentration after centrifugation. The inset is a Stern–Volmer calibration plot showing the ratio of the emission intensity (at 575 nm) in the absence of nanotubes (Fl^0) to the intensity in the presence of nanotubes (Fl). Stock CoMoCAT suspension's quenching efficiency = 98.8%. $R^2 = 0.998$.

looks similar, the efficiency of quenching for CoMoCAT SWCNTs (98.4%, $Fl^0/Fl = 62.9$) is found to be higher than that for HiPCO nanotubes (84.3%, $Fl^0/Fl = 6.4$). This suggests that the proportion of chiral forms that quench RB is higher in CoMoCAT than in HiPCO because the smaller diameter of CoMoCAT tubes are more dispersed than HiPCO tubes and consequently offer

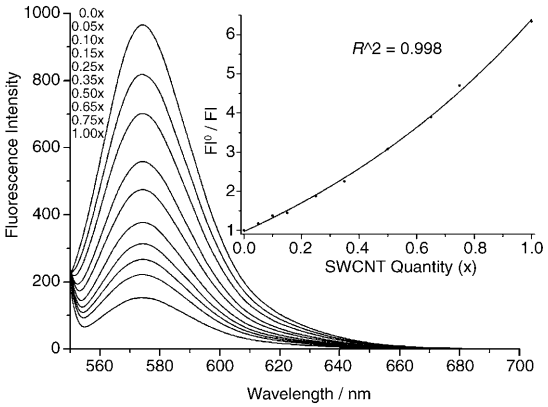

Figure 3. RB emission spectra of 0.42 μM (final concentration) in the presence of different quantities of HiPCO nanotubes (excitation wavelength: 535 nm). 1x refers to the starting concentration after centrifugation. The inset is a Stern–Volmer calibration plot showing the ratio of the emission intensity (at 575 nm) in the absence of nanotubes (Fl^0) to the intensity in the presence of nanotubes (Fl). Stock HiPCO suspension's quenching efficiency = 84.3%. $R^2 = 0.998$.

more surface area to which RB can bind. As a consequence, this arouses interest in the possibility to utilize RB quenching for identifying specific chiral forms in the dispersion.

Towards this aim, further experiments were performed to determine the quenching mechanism. As energy transfer has been proposed as the common mechanism for dye interactions with nanotubes,[9–11] we investigated the band-gap fluorescence (in the near-infrared) emitted from HiPCO and CoMoCAT nanotubes with and without RB. However, no significant fluorescence enhancement[9] could be detected upon addition of RB (see Supporting Information), suggesting that energy transfer is not the predominant mechanism here. In order to identify the quenching mechanism as being dynamic or static, fluorescence emission data were collected at different temperatures.[12] For this purpose, the spectra were recorded for various concentrations of CoMoCAT tubes after incubating the mixture at different temperatures (5°, 25° and 45 °C). Stern–Volmer plots obtained from these data are collected in Figure 4. It can be seen that the quenching efficiency correlates inversely with temperature, strongly supporting the static mode of quenching.[12] The quenching efficiency has reduced from 98.9% ($Fl^0/Fl = 89.3$) at 5 °C to 97.7% at 45 °C ($Fl^0/Fl = 43.5$). Based on this observation, a possible scenario for the quenching mechanism is shown in the inset of Figure 4. The increase in temperature favors the equilibrium to shift towards the non-complexed form of the dye and thereby reduces the fluorescence quenching efficiency. For dynamic/collisional quenching an opposite behavior would be expected, because at higher temperatures the collision probability would be increased leading to enhanced fluorescence.[12] Furthermore, the static complexation is consistent with the apparent small shift in the emission maxima of the PL spectra in Figures 1 to 3.

To gather further support for the proposed static quenching mechanism, the absorption spectrum of RB was monitored[11,22] with and without CoMoCAT SWCNTs as shown in Figure 5A. It is apparent that the absorption maximum of RB shows a clear

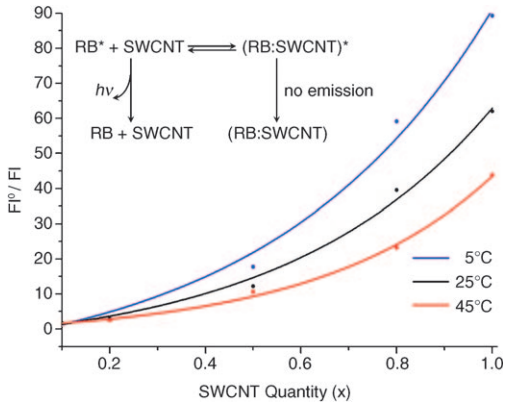

Figure 4. Stern–Volmer plots of RB quenching with CoMoCAT SWCNTs at different temperatures. All other parameters are similar to that in Figure 2. Quenching efficiency reduced from 98.9 to 97.7% as the temperature increased from 5 to 45 °C, indicative of a static quenching mechanism. The inset shows a possible scenario for the complexation and quenching of RB with nanotubes. RB*: excited dye, (RB:SWCNT) and (RB:SWCNT)*: complexed dye in the ground and excited states respectively.

red-shift from 554 nm to 562 nm upon addition to the tube suspension. This affirms the proposed model and suggests that a new complex with a different electronic structure is formed upon complexation. In order to study the effect of complexation on the electronic structure of the tubes, absorption spectra of the tubes were analyzed in the presence and absence of RB (Figure 5B). For this purpose, the absorption spectra of SWCNTs were obtained with RB as blank and corrected for changes in the electronic structure of complexed RB. It is apparent that the band marked **a** shows a clear blue shift (towards the position marked **b**), indicating that the complex formation is predominantly specific with just a few chiral forms [namely (6,5) and (6,4) tubes] that absorb light at ~580 nm.[23] By contrast the absorption of other chiral forms [such as (7,6), (7,5) and (8,3) corresponding to the band **c**, that absorb light at ~655 nm] in the presence of RB shows only a weak shift or remains almost unaffected.[23] The red shift in RB absorption and the concomitant blue shift in the absorption of specific chiral forms are consistent with the occurrence of photoinduced electron transfer[12,24–26] that might be responsible for the formation of the ground-state complex. This motivates the possibility of using standard curves of RB-quenching (Figure 2) to quantify specific chiral forms in an unknown sample especially for biological applications, such as drug delivery.

Figures 6A and B present the same analysis as above for the HiPCO tubes. While the red-shift indicative of dye complexation and the electronic structure changes for the dye and the nanotubes are qualitatively similar, there are some subtle differences. The magnitude of the absorption intensities here are lower than that for the CoMoCAT spectra (compare Figure 5B) suggesting that the proportion of the tubes with the absorption band at position **a** are much lower. This is in agreement with the distribution of nanotubes mapped by photoluminescence excitation spectroscopy.[27,28] In addition this explains the higher quenching efficiency of CoMoCAT tubes in comparison to HiPCO (Figures 2 and 3).

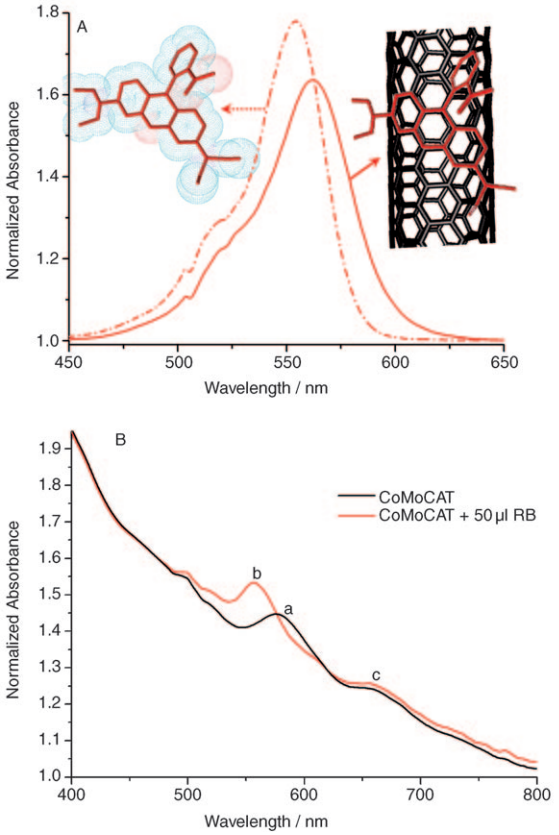

Figure 5. A) Absorption spectrum of RB without (dash dot line) and with (solid line) SWCNTs, displaying a red-shift of RB absorption maximum (from 554 nm to 562 nm) signifying complexation. CoMoCAT suspension was used as a blank to monitor the effect of nanotubes on the absorbance spectrum of RB. B) Corrected absorption spectrum of SWCNTs in the absence (black line) and presence (red line) of RB. RB solution was used as a blank, and the absorption measured and subsequently corrected for the change in the absorption of complexed RB. Specific chiral forms of nanotubes that absorb at position **a** are found to be blue-shifted in the presence of RB to position **b**, signifying complex formation. The tubes that absorb at position **c** show a weak or almost no complexation with RB.

Specific complexation between SWCNTs and RB was subsequently used to remove suspended non-tubular carbon nanostructures (amorphous carbon, fullerenes etc) and to enrich the suspension with specific chiral forms. Such partial purification was achieved by complex dependent precipitation of specific chiral forms, by centrifugation enhanced precipitation of dye-nanotube complex, while the non complexing nanomaterials remained in the supernatant. The absorbance of the resuspended pellet (after washing to remove RB) was analyzed. Figures 7A and B show that non-tubular nanostructures that absorb light from 200–400 nm[29] are significantly reduced upon complex dependent precipitation (position **a** in Figure 8). The absorption peaks related to specific chiral forms [such as (6,4) and (6,5) that are expected to complex with RB] remain unchanged (positions **b** in the insets of Figure 7) because they have been extracted from the original suspension by RB. In contrast, the absorbance related to other chiral forms [such as (7,5) and (7,6) that are not expected to complex with RB] have been reduced (positions **c** in the insets of Figure 7) since they remained in the supernatant.

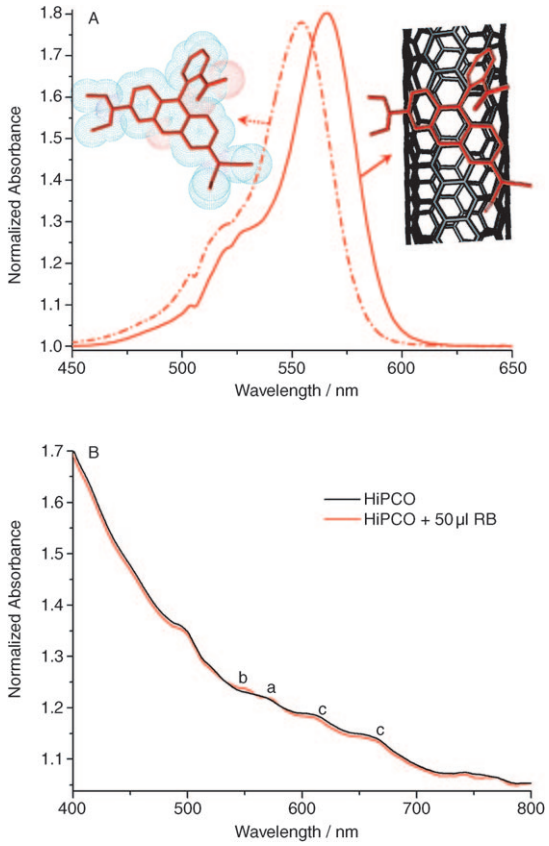

Figure 6. A) Absorption spectrum of RB without (dash dot line) and with (solid line) SWCNTs, displaying a red-shift of RB absorption maximum (from 554 nm to 566 nm) signifying complexation. HiPCO suspension was used as a blank to monitor the effect of nanotubes on the absorbance spectrum of RB. B) Absorption spectrum of SWCNTs in the absence (black line) and presence (red line) of RB. RB solution was used as a blank, and the absorption measured and subsequently corrected for the change in the absorption of complexed RB. Specific chiral forms of nanotubes that absorb at position **a** are found to be slightly blue-shifted in the presence of RB to position **b**, signifying complex formation. The tubes that absorb at position **c** show a weak or almost no complexation with RB.

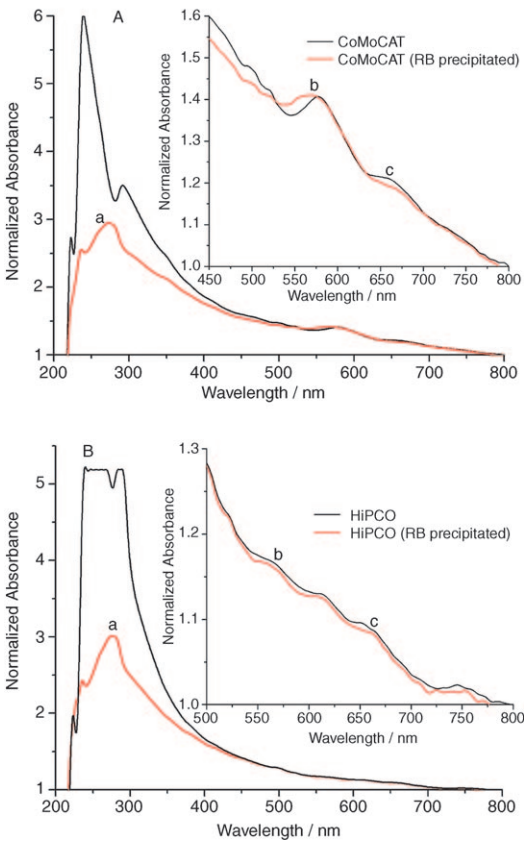

Figure 7. Absorption spectra of CoMoCAT (A) and HiPCO (B) carbon nanotubes before (red) and after (black) RB precipitation. Position a shows the reduction of non-tubular nanostructures upon RB precipitation. The insets show that the quantity of some chiral forms that form complex with RB remained unchanged (position **b**), while the proportion of other chiral forms (position **c**) that do not form a complex is reduced.

The capability of RB to form a non-fluorescing complex with SWCNTs was subsequently utilized to image individual tubes trapped across electrodes on a Si/SiO_2 substrate. A representative sample is shown in the AFM image in Figure 8A. The sample was dipped in a RB solution and blown dry to obtain a thin layer of RB on the surface. Confocal fluorescence images as shown in Figure 8B were subsequently recorded on the samples. It is apparent that the thin nanotube bundle in Figure 8A can be clearly visualized due to the efficient quenching of the dye fluorescence by complex formation with the nanotubes.

In conclusion, we have shown that SWCNTs quench RB through a static mode of action by forming a stable ground state (non-fluorescing) complex. Such complexation has been successfully used for: 1) characterizing an unknown suspension of SWCNTs by identifying the presence of specific chiral forms, 2) generating standard curves of RB-quenching to quantify specific chiral forms in an unknown sample for biological applications, such as drug delivery, 3) partial purification of SWCNTs suspension by reducing the non-tubular carbon nanostructures and enriching the suspension with specific chiral form and 4) visualizing SWCNTs on substrates instead of AFM for routine work.

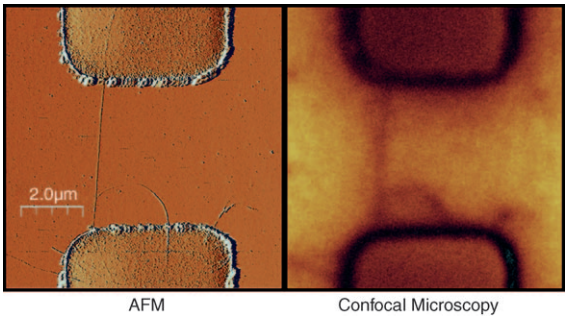

Figure 8. AFM (A) and confocal fluorescence (B) images of the same sample showing tube trapped across electrodes. The confocal image was recorded after leaving the sample in a solution of RB in ethanol. RB complexes to the nanotubes and hence the fluorescence is quenched along the tubes. This helps in the clear visualization of the tubes on a substrate.

Experimental Section

0.04 mg mL^{-1} HiPCO (High pressure pyrolysis of CO from Unidym, Inc.) and CoMoCAT (Co and Mo Catalyst process from SouthWest NanoTechnologies Inc.) SWCNTs were separately sonicated (SONOPULS Ultrasonic Homogenizer HD-3100) in 0.1% Triton-X-100 (Acros) for 40 sec with 1 sec impulse and 2 sec rest intervals. SWCNTs dispersions were centrifuged (ROTANTA 460 RS, Hettich) at 4637 g (4600 rpm) for 30 min, and the supernatant was used as the stock dispersion assuming that the final SWCNTs concentration is 1x. Diluted SWCNT dispersions (0.8x, 0.7x, 0.5x …) were freshly prepared before the experiments by mixing the stock dispersion with the 0.1% surfactant solution in appropriate ratios. No further sonication was used in the case of freshly prepared stock dispersion.

42 μM stock RB (Sigma) solution was prepared in 5% ethanol and 10 μl was added to 1.0 mL of blank (0.1% triton X-100) and sample (SWCNTs suspension) for Stern–Volmer calibration plot generation. The mixing of RB solutions and triton X-100 or SWCNTs suspension was performed just before the measurements. The fluorescence emission from solutions (in the visible range) in standard cuvettes (10 mm path length) containing only the dye solution and with added SWCNTs were measured using a standard luminescence spectrometer (PerkinElmer, LS50B), with 535 nm excitation wavelength instead of 554 nm to reduce overlap between excitation and emission spectra. Optical absorption spectra (UV and visible) were measured using NanoPhotometer (Implen). SWCNT photoluminescence spectra (near infra-red range) were collected using the HORIBA Jobin–Yvon IBH FL-322 Fluorolog 3 spectrometer with standard 10 mm path length cuvettes.

SWCNTs-RB complex formation was used for partial purification of SWCNTs by adding RB to the 1x CoMoCAT and HiPCO suspension to a 0.1 mM final concentration. The mixture was incubated for 2 h at room temperature, followed by centrifugation at 4637 g (4600 rpm) for 30 min. The pellet was washed 10 times with acetone to get rid of RB, dried and re-suspended in 0.1% triton X-100. The absorbance spectra were measured for the resuspended pellets.

SWCNTs were trapped by AC dielectrophoresis across electrodes located on a Si/SiO_2 substrate. Deposition parameters: 10 V (peak-to-peak-voltage) at 25 MHz for 10 sec. After trapping, the surfactant was removed by washing with acetone and isopropanol. AFM images were obtained on a Digital Instruments Dimension IV microscope.

Acknowledgements

This work was funded by the German Federal Ministry of Education and Research (BMBF) with the project ID O3X5516. We gratefully acknowledge the collaboration with Prof. Luisa De Cola and Dr. André Devaux (University of Münster) for help with the spectroscopic measurements.

Keywords: dyes/pigments · fluorescence spectroscopy · rhodamine B · static quenching · nanotubes

[1] M. C. Hersam, *Nat. Nanotechnol.* **2008**, *3*, 387.
[2] S. Iijima, *Nature* **1991**, *354*, 56.
[3] T. Guo, *J. Phys. Chem.* **1995**, *99*, 10694.
[4] M. José-Yacamán, *Appl. Phys. Lett.* **1993**, *62*, 657.
[5] P. Nikolaev, M. J. Bronikowski, R. K. Bradley, F. Rohmund, D. T. Colbert K. A. Smith, R. E. Smalley, *Chem. Phys. Lett.* **1999**, *313*, 91.
[6] B. Kitiyanan, W. E. Alvarez, J. H. Harwell, D. E. Resasco, *Chem. Phys. Lett.* **2000**, *317*, 497.
[7] R. Weisman, S. M. Bachilo, D. Tsyboulski, *Appl. Phys. A* **2004**, *78*, 1111.
[8] C. A. M. Seidel, A. Schulz, M. H. M. Sauer, *J. Phys. Chem.* **1996**, *100*, 5541.
[9] A. Ahmad, K. Kern, K. Balasubramanian, *ChemPhysChem* **2009**, *10*, 905.
[10] V. Biju, T. Itoh, Y. Baba, M. Ishikawa, *J. Phys. Chem. B* **2006**, *110*, 26068.
[11] K. Yanagi, K. Iakoubovskii, H. Matsui, H. Matsuzaki, H. Okamoto, Y. Miyata, Y. Maniwa, S. Kazaoui, N. Minami, H. Kataura, *J. Am. Chem. Soc.* **2007**, *129*, 4992.
[12] J. Lakowicz, *Principles of Fluorescence Spectroscopy, 2nd ed.*, Plenum, New York, **1999**.
[13] T. Förster, *Ann. Phys.* **1948**, *437*, 55.
[14] D. L. Dexter, *J. Phys. Chem.* **1953**, *21*, 836.
[15] L. Stryer, *Annu. Rev. Biochem.* **1978**, *47*, 819.
[16] M. K. Johansson, R. M. Cook, *Chem. Eur. J.* **2003**, *9*, 3466.
[17] J. E. Fischer, *Acc. Chem. Res.* **2002**, *35*, 1079.
[18] D. M. Guldi, G. M. A. Rahman, V. Sgobba, C. Ehli, *Chem. Soc. Rev.* **2006**, *35*, 471.
[19] M. Iurlo, D. Paolucci, M. Marcaccio, F. Paolucci, *Chem. Commun.* **2008**, 4867.
[20] V. Sgobba, D. M. Guldi, *Chem. Soc. Rev.* **2009**, *38*, 165.
[21] O. Stern, M. Volmer, *Phys. Z.* **1919**, *20*, 183.
[22] T. G. Hedderman, S. M. Keogh, G. Chambers, H. J. Byrne, *J. Phys. Chem. B* **2004**, *108*, 18860.
[23] R. B. Weisman, S. M. Bachilo, *Nano Lett.* **2003**, *3*, 1235.
[24] H. Lin, Y. Weng, H. Huang, Q. He, M. Zheng, F. Bai, *Appl. Phys. Lett.* **2004**, *84*, 2980.
[25] T. Hasobe, S. Fukuzimi, P. V. Kamat, *J. Phys. Chem. B* **2006**, *110*, 25477.
[26] F. D'Souza, R. Chitta, A. S. D. Sandanayaka, N. K. Subbaiyan, Y. Araki, O. Ito, *J. Am. Chem. Soc.* **2007**, *129*, 15865.
[27] S. M. Bachilo, M. S. Strano, C. Kittrell, R. H. Hauge, R. E. Smalley, R. B. Weisman, *Science* **2002**, *298*, 2361.
[28] A. Nish, J.-Y. Hwang, J. Doig, R. J. Nicholas, *Nat. Nanotechnol.* **2007**, *2*, 640.
[29] H. Kataura, Y. Kumazawa, Y. Maniwa, I. Umezu, S. Suzuki, Y. Ohtsuka, Y. Achiba, *Synth. Met.* **1999**, *103*, 2555.

Received: March 30, 2009
Revised: May 27, 2009
Published online on July 23, 2009

